Emiss. Control Sci. Technol. (2015) 1:98–107
DOI 10.1007/s40825-014-0003-6

A SCR Model Calibration Approach with Spatially Resolved Measurements and NH_3 Storage Distributions

Xiaobo Song · Gordon G. Parker · John H. Johnson · Jeffrey D. Naber · Josh A. Pihl

Received: 31 October 2014 / Accepted: 13 November 2014 / Published online: 27 November 2014

Abstract The selective catalytic reduction (SCR) is a technology used for reducing NO_x emissions in the heavy-duty diesel (HDD) engine exhaust. In this study, the spatially resolved capillary inlet infrared spectroscopy (Spaci-IR) technique was used to study the gas concentration and NH_3 storage distributions in a SCR catalyst, and to provide data for developing a SCR model to analyze the axial gaseous concentration and axial distributions of NH_3 storage. A two-site SCR model is described for simulating the reaction mechanisms. The model equations and a calculation method was developed using the Spaci-IR measurements to determine the NH_3 storage capacity and the relationships between certain kinetic parameters of the model. A calibration approach was then applied for tuning the kinetic parameters using the spatial gaseous measurements and calculated NH_3 storage as a function of axial position instead of inlet and outlet gaseous concentrations of NO, NO_2, and NH_3. The equations and the approach for determining the NH_3 storage capacity of the catalyst and a method of dividing the NH_3 storage capacity between the two storage sites are presented. It was determined that the kinetic parameters of the adsorption and desorption reactions have to follow certain relationships for the model to simulate the experimental data. The modeling results served as a basis for developing full model calibrations to SCR lab reactor and engine data and state estimator development as described in the references (Song et al. 2013a, b; Surenahalli et al. 2013).

X. Song (✉) · G. G. Parker · J. H. Johnson · J. D. Naber
Department of Mechanical Engineering-Engineering Mechanics, Michigan Technological University, 1400 Townsend Dr, Houghton, MI 49931, USA
e-mail: xiaobos@mtu.edu

J. A. Pihl
Oak Ridge National Laboratory, 1 Bethel Valley Rd, Oak Ridge, TN 37831, USA

Keywords Aftertreatment · Selective catalytic reduction (SCR) · Spaci-IR · NO_x reduction · SCR model

Nomenclature

ε	Void fraction of the catalyst channel [–]
u	Gas flow velocity [m/s]
β	Mass transfer coefficient [m/s]
A_g	Geometric surface area [1/s]
C	Mole fraction of species [–]
C_g	Mole fraction of species in gas phase [–]
C_s	Concentration of species in surface phase [–]
Ω	NH_3 storage capacity of the catalyst [gmol/m^3]
$\Omega_{A,}$	NH_3 storage capacity of the first site [gmol/m^3]
$\Omega_{B,}$	NH_3 storage capacity of the second site [gmol/m^3]
Ω_i	NH_3 storage at different temperatures [gmol/m^3]
Θ	NH_3 coverage fraction [–]
R	Reaction rate of the global reactions [1/s]
k	Reaction rate constant
A	Arrhenius form pre-exponential factor
E	Arrhenius form activation energy [kJ/gmol]
T	Temperature [K]
η_{O2}	The mole fraction of O_2[–]

1 Introduction

As emission regulations for diesel engines become increasingly stringent, urea-SCR has emerged as the dominant NO_x reduction technology for HDD vehicles [11]. Urea-SCR reduces NO_x through a series of chemical reactions on the catalytic surface between NO_x and adsorbed NH_3. The NH_3 is generated from decomposition of injected urea water solution called diesel exhaust fluid (DEF) in the USA. Among different SCR technologies, zeolite-based SCR is an accepted solution for SCR catalytic materials because of its low

temperature performance and thermal durability [2, 13, 14]. The NO_x reduction efficiency of the SCR needs to be 95 % or higher, with minimal NH_3 slip, to meet 2013 emission regulations [12]. At the same time, low urea usage is desirable for reducing operating costs.

In order to understand the characteristics and improve the performance of the SCR system to meet the requirements above, both extensive experimental and modeling studies are imperative. An accurate high fidelity model is valuable for more efficiently designing the SCR system, on-vehicle control system and diagnostic functions. The characteristics and performance of Cu-zeolite and Fe-zeolite catalysts have been studied through both engine and reactor experiments [3, 5, 14]. Numerous SCR models and kinetic studies have also been published for different formulations including Cu-zeolite and Fe-zeolite catalysts [6, 8, 17, 20, 24]. However, most of the modeling studies focused on only the SCR inlet and outlet emission measurements without considering the spatial measurements in the channels. Very limited modeling studies have considered the gas concentration measurements at different axial locations of the catalyst channel. The SCR models were normally calibrated to match the outlet experimental measurements using the inlet measurements as input. A model that can accurately predict the catalyst outlet concentrations may not meet the requirements of analysis lead design or control development if it was not able to correctly predict the catalyst internal concentration and NH_3 storage distribution. The recently developed spatially resolved capillary inlet infrared spectroscopy (Spaci-IR) technique [9, 10, 16] provides opportunities for studying the axially resolved gas concentrations and NH_3 storage distributions in the SCR channel, and the opportunities for improving the SCR model calibration process in order to correctly predict the SCR kinetics and catalyst internal states. A few limited modeling studies have considered the measurements at different axial locations of the catalyst channel [1].

This study aims to introduce the Spaci-IR technique and measurements as well as to develop a new model calibration approach with the Spaci-IR measurements. Such approach has not been published elsewhere and could be used for different SCR catalysts. The developed model calibration severed as a basis for developing a full model calibration with SCR lab reactor as well as engine data. In this study, a Cu-zeolite SCR core was tested in a flow reactor using the Spaci-IR technique. The Spaci-IR approach allowed measurements of gas concentrations axially within the core sample and computation of axial distributions of ammonia storage. A two-site one-dimensional SCR model with mass transfer and SCR reactions between stored NH_3 and other species was calibrated to the Spaci-IR experimental results by identifying the key parameters of the model, including NH_3 storage capacity, activation energies and pre-exponential constants for each SCR reaction. The Spaci-IR experiments and model calibration were performed on a degreened catalyst. The aging effects were not considered.

The SCR model has two storage sites as described in refs. [21, 22]. NH_3 adsorption and desorption take place on both sites, but SCR reactions only occur on the first site. The storage capacities of both sites were quantified to fit the experimental data by comparing the simulation results of one and two site models, with the experimental results. Activation energies and pre-exponential constants of key SCR reactions were calculated using axial gradients of gaseous concentrations and were further tuned using an optimization process. The calibrated SCR model was able to correctly predict both spatially resolved concentrations and NH_3 storage distributions under NH_3 saturation and NO_x SCR reaction conditions. The model calibration developed in this study provided a basis to further develop a full model calibration to lab reactor data under various conditions as well as a full model calibration to SCR engine data under both steady-state and transient conditions.

2 Spaci-IR Experiments

This investigation focused on a commercial Cu-exchanged zeolite SCR catalyst sampled from the production SCR of a 2010 Cummins ISB engine. The catalyst has a cell density of 400 cells per square inch (CPSI) and wall thickness of 4 mil. A 5-cm-long, 2-cm diameter core sample was cut from the face of the catalyst brick. The core sample was hydrothermally treated in a laboratory furnace at 700 °C for 4 h under a flow of 20 % O_2, 4.5 % H_2O, balance N_2 prior to the experimental evaluation.

Experiments were conducted in an automated flow reactor at Oak Ridge National Laboratory (ORNL) [19]. A schematic of the experimental setup is shown in Fig. 1. The flow reactor uses synthetic exhaust mixture to probe specific functions and properties of catalytic materials. Gas compositions were mixed from compressed gas cylinders using mass flow controllers. Water vapor was introduced through an HPLC pump and a custom capillary injection vaporizer system. Two four-way pneumatically actuated switching valves directed the flow of NH_3 and NO_x either to the reactor or to an exhaust line, creating approximately stepwise changes (0.5 s transient time) in inlet gas composition. All of the stainless steel reactor gas lines (6.4 mm diameter) were heated to 200 °C to prevent water condensation, adsorption of NH_3, and formation of NH_4NO_3 [4]. The SCR core sample was wrapped in fiberglass strands and loaded in a 2.5-cm diameter quartz tube. The upstream portion of the quartz tube was filled with 3-mm quartz chips to increase heat transfer to the inlet gas stream and improve temperature uniformity.

The quartz tube was fitted with graphite ferrules and custom stainless steel end caps that connect to the reactor gas

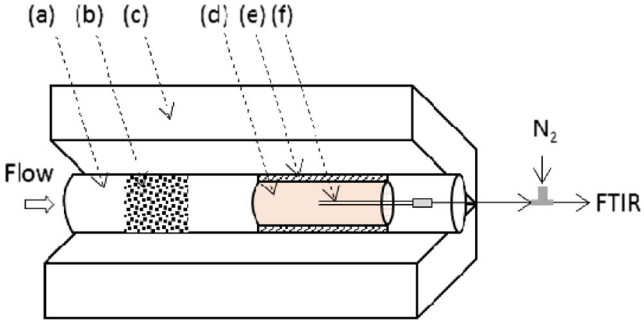

Fig. 1 A Schematic of the Spaci-IR experimental setup: **a** quartz tube, **b** quartz chips, **c** furnace, **d** catalyst core sample, **e** fiberglass strands, **f** capillaries

lines and provide inlet ports for thermocouples, pressure transducers, and sampling lines. The quartz tube assembly was placed in a tube furnace to precisely control the catalyst temperature. Type K thermocouples (0.5 mm diameter) were deployed 5 mm upstream, 5 mm downstream, and at the midpoint inside the SCR core sample to monitor catalyst temperatures. Reactor pressures were monitored with silicon-diaphragm absolute pressure transducers. A custom LabVIEW interface provided automated data acquisition and system control.

To measure gas concentrations and surface NH_3 inventories inside the SCR core sample, the Spaci-IR approach developed by Luo and coworkers [15] was modified. The approach uses a capillary inserted in a substrate channel to sample the gas from a particular axial location. The capillary can be translated within the channel to develop axially resolved maps of gas composition. A dilution flow is added to the sample gas stream at the outlet of the reactor to reduce gas transient times, and the diluted flow goes to an FTIR spectrometer (MKS Instruments Multi-gas 2030HS) for analysis. To improve both the transient response characteristics and the accuracy of the concentration measurements, the sample flow rate was increased by: (1) deploying two sampling capillaries (0.68 mm outer diameter) in neighboring substrate channels, and (2) increasing the reactor pressure to 1.1 bar with a downstream needle valve. A dilution ratio of 10:1 was found to be able to yield the optimal balance between temporal response and gas concentration resolution. A higher dilution ratio would increase the sampling flow rate, thus reduce the response time of the FTIR to enable better transient measurements. However, it would also decrease the gas concentrations measured by the FTIR and the measurement error will be further amplified when calculating the actual gas concentrations before dilution. A lower dilution ratio would have the opposite effects. The actual dilution ratio was calculated by comparing the measured CO_2 concentration with the known CO_2 feed concentration and it was used to correct the sample gas concentrations back to their undiluted values. A total of seven axial locations were measured. The measured points are located at 0.05, 0.1, 0.2, 0.3, 0.4, 0.6, and 0.8 of the channel length.

The experimental protocol as summarized in Table 1 was designed to measure spatially resolved gas concentrations and surface NH_3 inventory under three steady-state operating conditions: complete NH_3 saturation (in the presence of O_2), NO+NH_3 (standard) SCR, and NO_x+NH_3 (fast) SCR. The step changes in the inlet gas concentrations of the experimental protocol are shown in Fig. 2. For each step, operating conditions were held constant until the measured gas concentrations reached a steady state. Steps with NH_3 in the feed (steps 2, 4, and 7) were immediately followed by an inventory measurement step in which NH_3 was turned off while NO_x continued flowing (steps 5 and 8) or was turned on (step 3). Total NH_3 inventory was calculated by adding the desorbed NH_3 to the amount of incoming NO_x converted by stored NH_3. After the protocol was completed at one position within the substrate channel, the capillaries were moved to a different position, and the protocol was run again. This process was repeated until the concentrations were mapped across the length of the SCR core (a total of eight axial positions including one 0.4 cm upstream of the catalyst to measure inlet composition). The entire protocol was run at three different temperatures (250, 300, 350 °C). The temperature range is typical for running SCR reactor data although in the future data at 200, 400, and 450 °C would be of interest for applying the approaches developed in this paper. The Spaci-IR data will be shown along with the model simulation results for comparison purpose.

All experiments were run at a nominal space velocity of 60,000 h^{-1} based on flows at standard conditions and total SCR core sample volume. However, during calculation and analysis of the NH_3 storage distributions, it was determined that the Spaci-IR approach implemented for this study introduced sampling artifacts. These artifacts became apparent when the saturation NH_3 storage capacities calculated from

Table 1 Details of each step of the Spaci-IR test protocol

Step	Description	NO ppm	NO_2 ppm	NH_3 ppm
1	Stabilize	0	0	0
2	NH_3 adsorption	0	0	350
3	NH_3 inventory: NO_2/NO_x=0.5	175	175	0
4	NH_3/NO_x=1.0; NO_2/NO_x=0.5	175	175	350
5	NH_3 inventory: NO_2/NO_x=0.5	175	175	0
6	stabilize NO: NO_2/NO_x=0.0	350	0	0
7	NH_3/NO_x=1.0; NO_2/NO_x=0.0	350	0	350
8	NH_3 inventory: NO_2/NO_x=0.0	350	0	0
9	Clean: NO_2/NO_x=0.5	175	175	0

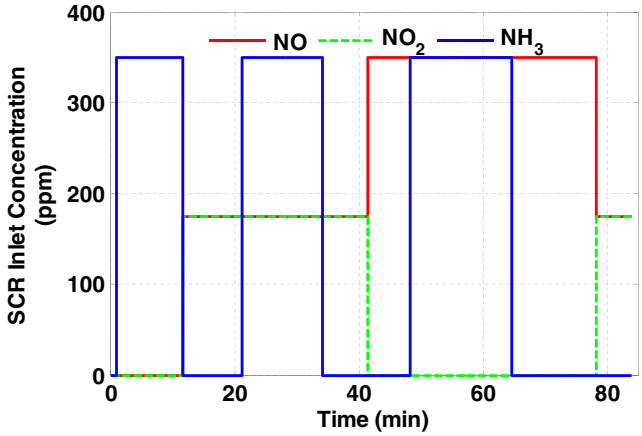

Fig. 2 Experimental protocol showing the changes in the inlet gas concentrations of the Spaci-IR reactor experiments

the Spaci-IR data were consistently lower than those measured on the same catalyst with effluent measurements (without the Spaci-IR sampling system). The discrepancy in measured NH_3 storage was most likely due to anomalously high flows along the channels that contained the sampling capillaries. The capillaries provided a reduced backpressure flow path, pulling a higher flow into the sampled channels. By comparing the NH_3 storage measured with Spaci-IR to the NH_3 storage measured with traditional effluent measurements, it was determined that the actual space velocity within the channels was 69,000 h^{-1}. This corrected value was used in all subsequent calculations and modeling.

3 SCR Model Review

The SCR model that will be used in the analysis of the Spaci-IR data was developed and calibrated using inlet and outlet NH_3, NO_2, and NO concentration data for the Cu-zeolite SCR as described in refs. [21, 22]. The model is briefly reviewed so it can be used in the calculation and calibration process. It is a two-site one-dimensional single channel model with an isothermal assumption. It was assumed that the channel of the SCR is evenly divided into ten elements in the axial direction. Each element had eight states. Three states were for bulk gas concentrations for NH_3, NO, and NO_2. Three more states were used for the surface layer gas concentration of the same three species. The seventh and eighth states were for NH_3 storage. The model had two separate sites supporting NH_3 adsorption and desorption reactions but with only the first site supporting all chemical reactions included in the model. The second storage site was needed empirically in order to develop an accurate model that simulates the experimental data. The reactions included in the model are given in the equations from R1 to R12. S_1 and S_2 represent the two storage sites. $NH^*_{3,1}$ and $NH^*_{3,2}$ represent the NH_3 stored on the first and second site separately. R7 was added into the model to simulate the NH_3 over-consumption observed in the flow reactor data under NO+NH_3 reaction conditions [22].

$$NH_3 + S_1 \rightarrow NH^*_{3,1} \quad \text{(R1)}$$

$$NH^*_{3,1} \rightarrow NH_3 + S_1 \quad \text{(R2)}$$

$$NH_3 + S_2 \rightarrow NH^*_{3,2} \quad \text{(R3)}$$

$$NH^*_{3,2} \rightarrow NH_3 + S_2 \quad \text{(R4)}$$

$$4NH^*_{3,1} + 3O_2 \rightarrow 2N_2 + 6H_2O \quad \text{(R5)}$$

$$4NH^*_{3,1} + 4NO + O_2 \rightarrow 4N_2 + 6H_2O \quad \text{(R6)}$$

$$5NH^*_{3,1} + 3NO + 9/4\ O_2 \rightarrow 4N_2 + 15/2\ H_2O \quad \text{(R7)}$$

$$4NH^*_{3,1} + 2NO + 2\ NO_2 \rightarrow 4N_2 + 6H_2O \quad \text{(R8)}$$

$$4NH^*_{3,1} + 3\ NO_2 \rightarrow 7/2N_2 + 6H_2O \quad \text{(R9)}$$

$$2\ NO + O_2 \leftrightarrow 2\ NO_2 \quad \text{(R10)}$$

$$6NH^*_{3,1} + 8\ NO_2 \rightarrow 7N_2O + 9H_2O \quad \text{(R11)}$$

$$4\ NH^*_{3,1} + 5\ O_2 \rightarrow 4\ NO + 6\ H_2O \quad \text{(R12)}$$

The mass balance equation for each axial element of the model is given as Eq. 1. The governing equation for

transfer between gas and surface phase is given as Eq. 2. The "d/dt" terms were used in the model equations to allow exploration of transient behaviors. The storage equation for the NH_3 storage site is shown as Eq. 3 [22].

$$\varepsilon\frac{\partial C_{g,i}}{\partial t} = -u\frac{\partial C_{g,i}}{\partial x} - \beta_i A_g\left(C_{g,i} - C_{s,i}\right) \tag{1}$$

$$(1-\varepsilon)\frac{\partial C_{s,i}}{\partial t} = \beta_i A_g\left(C_{g,i} - C_{s,i}\right) - \sum_j N_{i,j} R_j \tag{2}$$

$$\Omega_m \theta_m = R_{\mathrm{Ads},m} - R_{\mathrm{Des},m} - \sum_j n_j R_j \tag{3}$$

In the equations, ε is the void fraction of the catalyst, u is the velocity of the exhaust flowing through the catalyst, A_g is the geometric surface area and β_i is the mass transfer coefficient introduced in ref. [22]. C_g and C_s are the gas phase and surface phase gaseous concentrations. R is the reaction rate for each reaction included in the model. The reaction rate calculations are introduced in reference [22]. The subscript i represents the ith gas species, j represents the jth reaction taking place on the catalytic surface, m represents the mth storage site, n is the order of each reaction.

4 Model Calibration Development with Spaci-IR Data

As can be seen from the SCR reaction equations, the NH_3 stored on the catalyst participates in all SCR reactions. As a result, the NH_3 storage capacities of each model site (Ω_A and Ω_B) are key parameters that need to be identified. The total NH_3 storage capacity of the catalyst can be calculated by integrating the NO_x reduced by stored NH_3 during step 3 of the protocol. However, since there were two storage sites in the model, how to separate the total storage capacity between each site became a unique problem to solve. The gas phase concentrations were assumed to be equal to the surface phase concentrations in this analysis.

For the purpose of simplifying the calculation and verification, a one-site model was used to compute the total ammonia storage. The steady-state portion of the experimental data at step 2, after NH_3 saturation, was used for the analysis. The time rate of change of stored NH_3 was zero and the reaction rate of the adsorption reaction was equal to that of the desorption reaction. This leads to Eq. 4

$$\begin{aligned} R_{\mathrm{ads}} &= k_{\mathrm{ads},i} C_{\mathrm{NH_3},i}(1-\theta_i)\,\Omega \\ &= R_{\mathrm{des}} = k_{\mathrm{des},i}\theta_i \Omega \end{aligned} \tag{4}$$

$$k_j = A_j \exp\left(-E_j/RT_i\right) \tag{5}$$

Where the subscript i represents the ith test temperature (250, 300, or 350 °C) and j is reaction index. The quantity k is the reaction rate constant, C is the gas concentration, θ is the NH_3 storage site coverage fraction, and Ω is the storage capacity. The calculation of reaction rate constant k is given in Eq. 5. After substituting and re-arrangement of the equations, Eq. 6 can be easily obtained.

$$\begin{aligned} \ln\left(\frac{A_{\mathrm{ads}}}{A_{\mathrm{des}}}\right) - \frac{(E_{\mathrm{ads}} - E_{\mathrm{des}})}{RT_i} &= \ln\left(\frac{\Omega_i}{C_{\mathrm{NH_3},i}}\right) \\ &\quad - \ln(\Omega - \Omega_i) \end{aligned} \tag{6}$$

$C_{NH3,i}$ was measured and Ω_i was determined from the experimental data for each temperature. Ω_i equals to the total storage capacity times the coverage fraction. The determined Ω_i for 250, 300, and 350 °C is shown in Fig. 3. The total volume of the SCR core sample was used for storage capacity calculations. A linear relationship between NH_3 storage and temperature without O_2 was reported in this temperature range for the same catalyst formulation [22]. The deviation from linear behavior in Fig. 3 is most likely due to NH_3 oxidation at 350 °C. To eliminate the effect of NH_3 oxidation, the line defined by the two lower temperature storage measurements was extrapolated to estimate an oxidation-corrected $\Omega_3^* = 43.1$ gmol/m^3. Using the measured NH_3 concentrations and calculated NH_3 inventories leaves three unknowns in Eq. 6: A_{ads}/A_{des}, $E_{ads}-E_{des}$, and the storage capacity Ω. After substituting the known parameters for each temperature, a set of three equations was available to solve for the three unknowns. One meaningful solution was Ω=108 gmol/m^3, $A_{ads}/A_{des}=2.84\times10^{-2}$, and $E_{ads}-E_{des}=-4.13\times10^4$ J/gmol. The NH_3 adsorption reaction is typically assumed to be non-activated (having an activation energy of zero) [18]. As a result, the activation energy for the desorption reaction is equal to 4.13×10^4 J/gmol.

The NH_3 oxidation at 350 °C was used to calculate the relationship between the reaction rate constant of R1 and R5

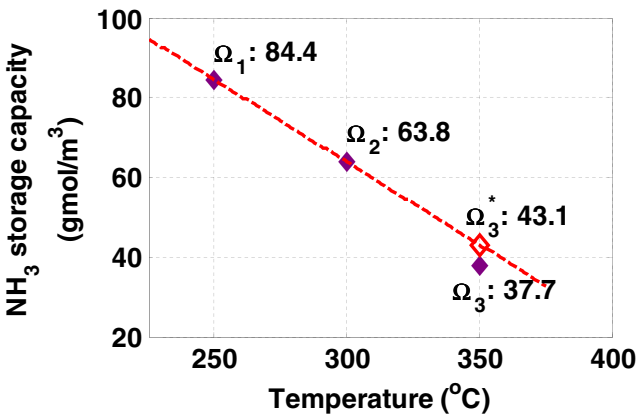

Fig. 3 NH_3 storage at temperatures of 250, 300, and 350 °C

by solving Eq. 7 which shows the reaction rate calculation of R5 and Eq. 3 with reactions of adsorption, desorption and NH_3 oxidation. The calculation results showed that $k_{ads}/k_{oxi1} = 1.63$ at the temperature of 350 °C.

$$R_{oxi1} = 4 \cdot k_{oxi1,3} \eta_{o2} \Omega_3 / \Omega \tag{7}$$

Because significant NO was not observed under the conditions with NH_3 and O_2 in the feed for all temperatures, the NH_3 oxidation to NO (R12) was not considered. Only NH_3 oxidation to N_2 (R5) was considered in the calibration process.

The next step was to calculate the activation energy and pre-exponential constant of the fast SCR reaction using steady-state portions of steps 4 and 5 of the protocol. Fast SCR reaction R8 was assumed to be dominant with a NO_2/NO_x ratio equal to 0.5, so other SCR reactions were not considered. Re-arranging Eqs. 1, 2, and 3 under these conditions yields Eq. 8. R_{fst} is the reaction rate of R8 shown as Eq. 9.

$$\frac{\partial C_{g,NH_3}}{2\partial x} = \frac{\partial C_{g,NO}}{\partial x} = \frac{\partial C_{g,NO_2}}{\partial x} - 2\frac{R_{fst}}{u} \tag{8}$$

$$R_{fst} = k_{fst} C_{NO,s} C_{NO_2,s} \Omega \theta \tag{9}$$

Axially resolved measurements of NH_3, NO, and NO_2 provided opportunities for calculating the fast SCR reaction rate constants through Eq. 8 and 9. k_{fst} on each axial element (divided by two axial measurement locations) was calculated using the axial measurements under each temperature for NH_3, NO, and NO_2 respectively. The calculated k_{fst} values at three temperatures for each element were then plotted in Arrhenius form as shown in Fig. 4 for the purpose of determining the activation energy and pre-exponential constant. Only the reaction rate constants on the first six axial elements were shown because low concentration and storage on the axial elements 7 and 8 caused larger uncertainties in the calculation results. The averaged slope of the Arrhenius plot was used for the activation energy calculation. The resulting activation energy for the fast SCR reaction was $E_{fst} \cong 5.38 \times 10^4$ J/gmol. The average of the pre-exponential A_{fst} at different axial locations was used for the model.

With the identification results presented above, the one-site SCR model was run with a set of parameters following the identified values and relationships between parameters. It was found that a one storage site model was not able to correctly simulate both axial gas concentrations and NH_3 storage distributions. One run with correct predictions of axial concentrations (as shown in Fig. 5) is given in Fig. 6. It implies that the model that can correctly predict the gaseous concentrations may not be able to accurately estimate the NH_3 storage at different axial locations of the SCR channel. It can be seen that the storage capacity at NH_3 saturation was correctly predicted. However, the NH_3 storage during the NO_x SCR condition was underestimated. The Spaci-IR data showed that the NH_3 is mainly stored on the first half the catalyst, while the simulation showed that the NH_3 storage is very low across the channel length. This was because the model overpredicts the rate of consumption of surface NH_3 by SCR reactions relative to the rate of NH_3 adsorption. Reducing the reaction rate of the fast SCR reaction (R8) by a magnitude without changing the NH_3 adsorption rate gives the correct prediction of the NH_3 storage under the NO_x SCR condition. However, this also results in underestimation of the NO_x conversion prediction at different axial positions of the channel. The conclusion is that it is not successful to predict both axial concentration and storage profiles with a single site model. The solution to correct the NH_3 storage prediction without affecting the gas concentration prediction was to add the second storage site which supported only NH_3 adsorption and desorption.

As shown in Fig. 6, the differences in NH_3 storage between model simulation and experimental results under NO_x SCR condition (ΔS1, ΔS2, and ΔS3) were considered to be the NH_3 stored on the second site. As a result, the NH_3 storage for each temperature on the second site was calculated to be 34.7,

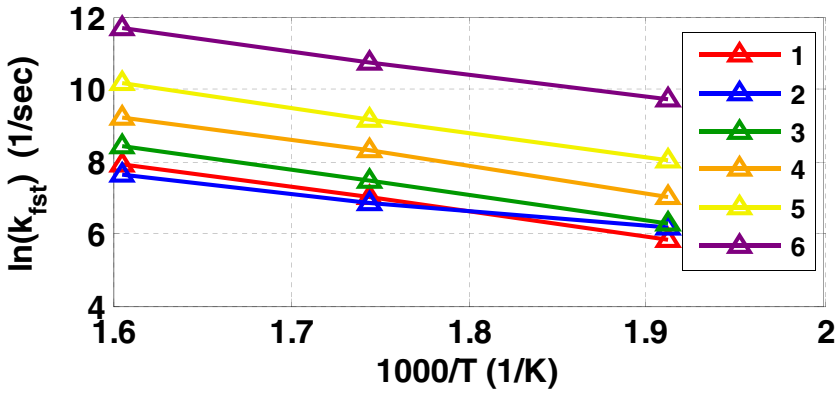

Fig. 4 Arrhenius form plot of the fast SCR reaction rate constant on each axial element

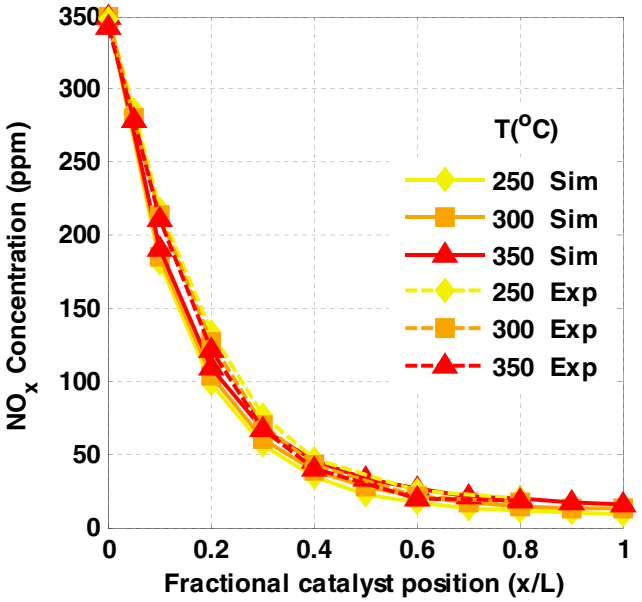

Fig. 5 One-site model simulated NO_x concentration at different axial locations at equilibrium state of NO_x SCR conditions compared to experimental results

21.1 and 7.6 gmol/m^3. By solving the set of equations derived from Eq. 6 for the second site at three temperatures, the storage capacity Ω_B, A_{ads2}/A_{des2}, and $E_{ads2}-E_{des2}$ can be solved. The meaningful solution for this set of equations was Ω_B=39.1 gmol/m^3, $A_{ads2}/A_{des2}=1.66\times10^{-6}$, and $E_{ads2}-E_{des2}=-8.92\times10^4$ J/gmol. The adsorption reaction on the second site was once again considered as a non-activated reaction, and E_{ads2} was set to zero, resulting in $E_{des2}=8.92\times10^4$ J/gmol. However, adding the second site without reducing the NH_3 storage capacity of the first site resulted in overestimation of the NH_3 stored during the NH_3 saturation section of the test protocol. The NH_3 storage capacity of site 1 needs to be reduced after adding the second site. The two-site model with identified parameters above was run to determine how much NH_3 was actually stored on the second site. Then, the difference in NH_3 storage between the NH_3 stored on the second site and the experimentally found storage was considered to be the storage on the first site. Simulation results showed that about 39.5, 30.0, and 20.5 gmol/m^3 of NH_3 was stored on the second site under NH_3 saturation condition for 250, 300, and 350 °C, respectively. The differences between storage values on the second site and the experimentally found values shown in Fig. 3 were 44.9, 33.8, and 17.2 gmol/m^3 for 250, 300, and 350 °C respectively, and those values were considered as the NH_3 storage on the first site after adding the second site. Then, the storage capacity of the first site (Ω_A), A_{ads1}/A_{des1}, and $E_{ads1}-E_{des1}$ were also updated through re-solving the equation set derived from Eq. 6 for each temperature. The solution was: Ω_A=55.5 gmol/m^3, $A_{ads1}/A_{des1}=1.28\times10^{-2}$, $E_{ads1}-E_{des1}=-4.54\times10^4$ J/gmol. Again E_{ads1} was set to be zero. The identified storage capacities and the relationships between the adsorption and desorption kinetic parameters are given in Table 2.

5 Results and Discussion

After determining the storage parameters for each site, the model kinetic parameters of the remaining reactions taking place on the first site were updated following the parameter identification process presented in the previous section. A full model calibration was obtained by further optimizing the calculated model parameters against experimental measurements [21, 22]. The optimization method used a MATLAB "fmincon" function [7] to find the set of parameters which gave the smallest cost function value which was defined as the error between simulated NH_3, NO, and NO_2 concentrations and the experimental measurements. The cost function is given as Eq. 10.

$$\text{Cost}_i = \sum_{t_0}^{t_{end}} \left| C_{i,\text{Sim}} - C_{i,\text{Exp}} \right| / (t_{end} - t_0) \tag{10}$$

Cost_i is the cost function for gas species i (i = NO, NO_2, NH_3). t_0 and t_{end} are the start and stop time in seconds for the simulation. $C_{i,sim}$ and $C_{i,exp}$ are the model simulated and experimentally measured gas concentration for the gas species i respectively. The comparison between the model simulation

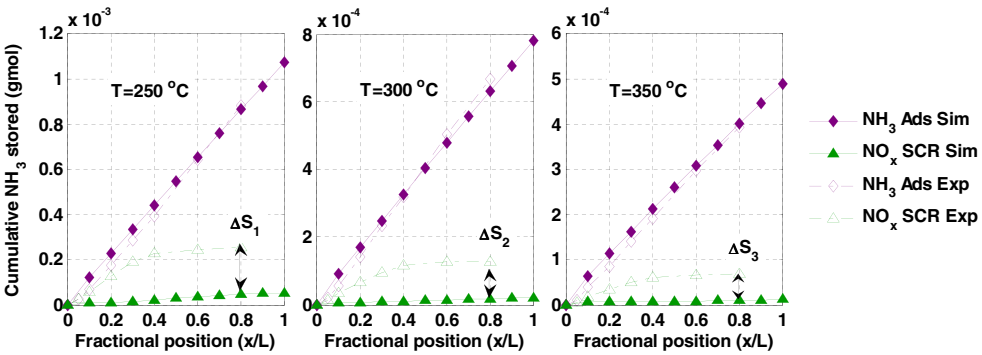

Fig. 6 One-site model simulated NH_3 storage distribution under NH_3 saturation and NO_x SCR conditions compared to experimental results for each test temperature

Table 2 Identified NH_3 storage capacities, A_{ads}/A_{des} and $E_{ads}-E_{des}$ for the storage sites of the two-site model

Parameter	Value	Units
Ω_A	55.5	gmol/m
Ω_B	39.1	gmol/m
A_{ads1}/A_{des1}	1.28×10^{-2}	None
$E_{ads1}-E_{des1}$	-4.54×10^{4}	J/gmol
A_{ads2}/A_{des2}	1.66×10^{-6}	None
$E_{ads2}-E_{des2}$	-8.92×10^{4}	J/gmol

results using the optimal parameters and the experimental data is given in Fig. 7. The top two plots show the comparison of axially resolved NO_x and NH_3 concentrations for each temperature between simulation and measurements under NO_x SCR condition of the protocol. The difference in concentrations between temperatures is not significant. This is because the SCR reactions at these test conditions are mainly limited by mass diffusion instead of temperature. The simulated concentrations also follow the same trend along the axial location. More than 90 % of the NO_x reduction took place in the first half of the catalyst length. There is no NH_3 available for NO_x reduction after fractional location of 0.6. However, a low concentration of NO_x is present after this position. The bottom three plots in Fig. 7 show the cumulative NH_3 stored on the catalyst at each axial measurement location for three temperatures under NH_3 saturation and NO_x SCR conditions of the protocol. The NH_3 stored under NH_3 saturation condition

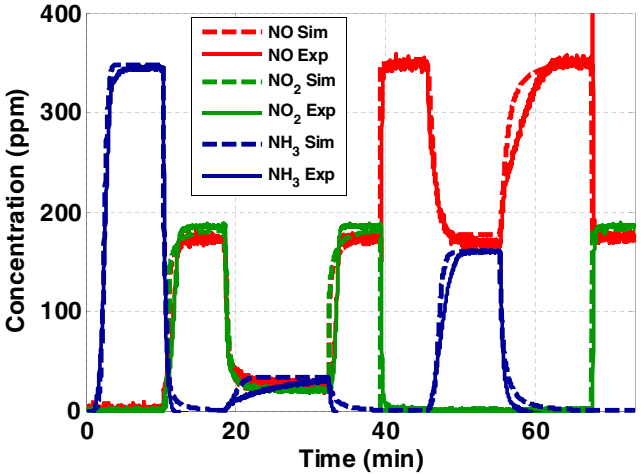

Fig. 8 Comparison of NO, NO_2, and NH_3 concentrations between model simulation and experimental measurements at axial position of 0.4 under temperature of 250 °C

shows a nearly linear increase along the axis for all three temperatures, as expected. The model can correctly predict this phenomenon except that it is slightly higher than the experimental results for the 350 °C data. The storage differences between NH_3 saturation and NO_x SCR conditions are due to the differences in the NH_3 concentration profile induced by the SCR reactions. For example, under steady-state NH_3 saturation conditions, the NH_3 concentration is the same throughout the catalyst, and the cumulative NH_3 stored

Fig. 7 Simulation results of the two-site model compared to experimental results

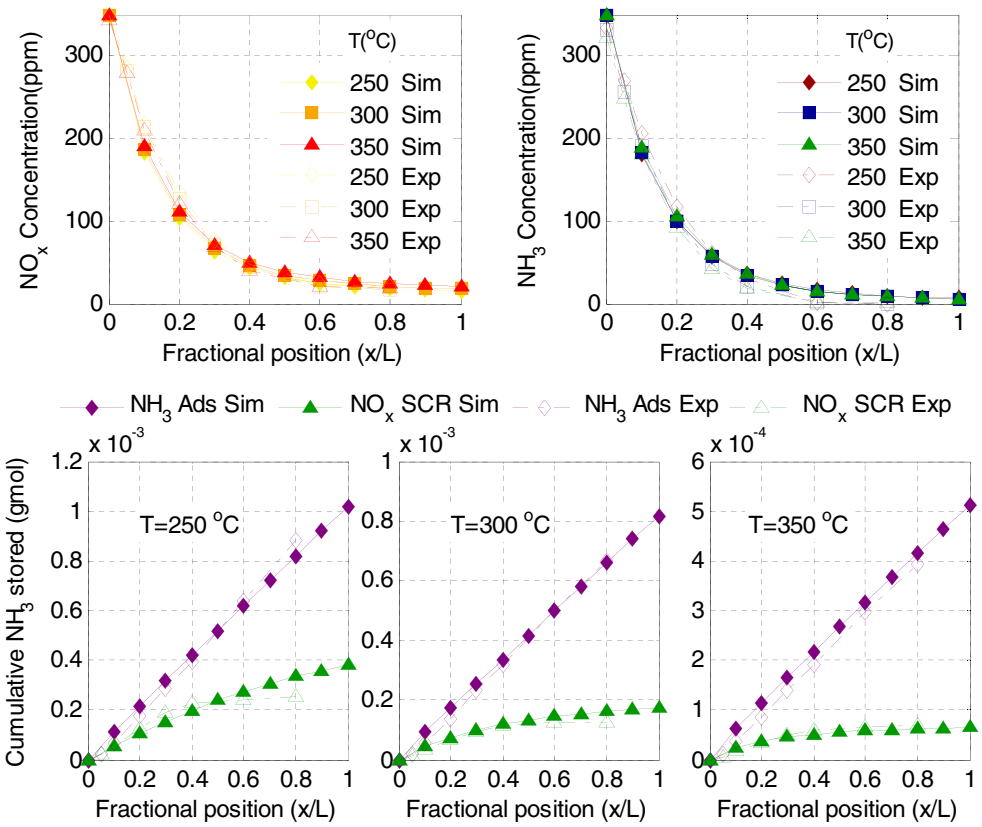

increases linearly with axial channel position as the cumulative number of upstream storage sites increases. However, when NO_x is included in the feed gas, NH_3 is consumed by the SCR reactions, and the NH_3 concentration decreases further into the substrate channel. Lower NH_3 concentrations result in lower NH_3 stored on the catalyst surface, so the cumulative NH_3 storage curves increase until it finally levels off at the point in the channel where all of the NH_3 has been consumed (about half way down the length of the channel) and there is none left to store. The model gives a slightly different trend for the NH_3 storage under SCR conditions at 250 °C. The measured cumulative NH_3 storage increases from inlet to 0.4 of the channel length and levels off. The simulation shows an increasing trend from inlet to outlet of the channel and gets higher than the measurements from 0.5 of the channel length with an over prediction of 30 % at 0.8 of the channel length. As shown in the NH_3 concentration plot of Fig. 7, the NH_3 is completely consumed after the 0.6 of the channel length in the reactor experiments. Thus, no NH_3 storage is observed after 0.6 of the channel length. However, the model still predicts about 10 ppm of NH_3 after 0.6 of the channel length and results in a low level of NH_3 storage from 0.6 position to the outlet. A comparison of the gas concentrations between the model predictions and the experimental measurements at the axial fractional position of 0.4 is shown in Fig. 8. It can be seen that the model predicted NO, NO_2, and NH_3 concentrations agree well with both steady-state and transient behaviors measured by the FTIR. The model simulation results agree with the experimental results for temperatures of 300 and 350 °C.

6 Summary and Conclusion

The Spaci-IR technique was useful for collecting data to study the gas concentrations as well as NH_3 storage distributions in a SCR catalyst, and to provide data for developing the SCR model. A one-site SCR model is not able to correctly predict both axially resolved concentrations and NH_3 storage distributions. Adding a second site which stores NH_3 but does not support other SCR reactiosns is necessary for improving the model performance. A solution for determining the NH_3 storage capacity of the catalyst and a unique method of dividing the NH_3 storage capacity between the two storage sites were presented. It was determined that the kinetic parameters of the adsorption and desorption reactions have to follow certain relationships for the model to simulate the experimental data. The identified relationships reduced the number of the model parameters that needed to be identified during the calibration process. The performance of the two-site SCR model with identified parameters and relationships was validated by comparing the simulation results to the reactor experimental results. The modeling results presented here served as a basis for developing model calibrations to both SCR reactor and engine data and state estimator [21–23].

Acknowledgments This material is based upon work supported by the Department of Energy National Energy Technology Laboratory under Award Number(s) DE-EE0000204.

References

1. Auvraya, X., Partridgeb, W., Choib, J.-S., Pihl, J., et al.: Kinetic modeling of NH_3-SCR over a supported Cu zeolite catalyst using axial species distribution measurements. Appl. Catal., B **2015**(163), 393–403 (2015)
2. Bartley, G.J., Chadwell, C.J., Kostek, T.M., Zhan, R.: SCR deactivation kinetics for model-based control and accelerated aging applications. SAE Tech. Pap. Ser. 2012-01-1077 (2012)
3. Cavataio, G., Kim, J.Y., Warner, J.R., Girard, J.W., Upadhyay, D., Lambert, C.K.: Development of emission transfer functions for predicting the deterioration of a Cu-Zeolite SCR catalyst. SAE Tech. Pap. Ser. 2009-01-1282 (2009)
4. Ciardelli, C., Nova, I., Tronconi, E., Chatterjee, D., Bandi-Konrad, B., Weibel, M., Krutzsch, B.: Reactivity of NO/NO_2-NH_3 SCR system for diesel exhaust aftertreatment: identification of the reaction network as a function of temperature and NO_2 feed content. Appl. Catal. B Environ. **2005**(70), 80–90 (2005)
5. Cloudt, R., Saenen, J., Eijnden, E.V.D., Rojer, C.: Virtual exhaust line for model-based diesel aftertreatment development. SAE Tech. Pap. Ser. 2010-01-0888 (2010)
6. Colombo, M., Koltsakis, G., Nova, I., Tronconi, E.: Modelling the ammonia adsorption-desorption process over an Fe-zeolite catalyst for SCR automotive applications. Catal. Today **188**(1), 42–52 (2011)
7. Devarakonda, M., Lee, J., Muntean, G., Pihl, J. et al.: 1D model of a copper exchanged small pore zeolite catalyst based on transient SCR protocol. SAE Tech. Pap. 2013-01-1578 (2013)
8. Devarakonda, M., Tonkyn, R., Lee, J.: Modeling species inhibition and competitive adsorption in urea-SCR Catalysts. SAE Tech. Pap. Ser. 2012-01-1295 (2012)
9. Henry, C., Kamasamudram, K., Currier, N., Yezerets, A.: Axially resolved performance of Cu-Zeolite SCR catalysts. SAE Tech. Pap. Ser. 2012-01-1084 (2012)
10. Hou, X., Epling, W.S., Schmieg, S.J., Li, W.: Cu-Zeolite SCR catalyst thermal deactivation studied with FTIR spatial resolution. SAE Tech. Pap. Ser. 2011-01-1138 (2011)
11. Johnson, T.V.: Diesel emission control in review. SAE Tech. Pap. Ser. 2007-01-0233 (2007)
12. Johnson, T.V.: Vehicular emissions in review. SAE Tech. Pap. Ser. 2012-01-0368 (2012)

13. Kamasamudram, K., Currier, N.W., Chen, X., Yezerets, A.: Overview of the practically important behaviors of zeolite-based urea-SCR catalysts, using compact experimental protocol. Catal. Today **2010**(151), 212–222 (2010)
14. Kamasamudram, K., Currier, N., Szailer, T., Yezerets, A.: Why Cu- and Fe-Zeolite SCR catalysts behave differently at low temperatures. SAE Tech. Pap. Ser. 2010-01-1182 (2010)
15. Luo, J.-Y., Hou, X., Wijayakoon, P., Schmieg, S.J., Li, W., Epling, W.S.: Spatially resolving SCR reactions over a Fe/zeolite catalyst. Appl. Catal., B **2011**(102), 110–119 (2011)
16. Luo, J.-Y., Oh, H., Henry, C., Epling, W.: Effect of C_3H_6 on selective catalytic reduction of NO_x by NH_3 over a Cu/zeolite catalyst: a mechanistic study. Appl. Catal., B **2012**(123–124), 296–305 (2012)
17. Markatou, P., Dai, J., Johansson, A., Wassim Klink, M.C., Watling, T.C., Tutuianu, M.: Fe-Zeolite SCR model development, validation and application. SAE Tech. Pap. Ser. 2011-01-1304 (2011)
18. Nova, I., Colombo, M., Tronconi, E., Schmeisse, V., Weibel, M.: The NH_3 inhibition effect in the standard SCR reaction over a commercial Fe-zeolite catalyst for diesel exhaust aftertreatment: an experimental and modeling study. SAE Tech. Pap. Ser. 2011-01-1319 (2011)
19. Pihl, J.A., Toops, T.J., Fisher, G.B., West, B.H.: Selective catalytic reduction of nitric oxide with ethanol/gasoline blends over a silver/alumina catalyst. Catal. Today **2014**(231), 46–55 (2014)
20. Sharifian, L., Wright, Y.M., Boulouchos, K., Elsener, M., Kröcher, O.: Transient simulation of NO_x reduction over a Fe-Zeolite catalyst in an NH_3-SCR system and study of the performance under different operating conditions. SAE Tech. Pap. Ser. 2011-01-2084 (2011)
21. Song, X., Naber, J., Johnson, J., Parker, G.: An experimental and modeling study of reaction kinetics for a Cu-Zeolite SCR catalyst based on engine experiments. SAE Tech. Pap. Ser. 2013-01-1054 (2013a)
22. Song, X., Parker, G., Johnson, J., Naber, J., Pihl, J.: A modeling study of SCR reaction kinetics from reactor experiments. SAE Tech. Pap. Ser. 2013-01-1576 (2013b)
23. Surenahalli, H., Parker, G., Johnson, J.: Extended Kalman filter estimator for NH_3 storage, NO, NO_2 and NH_3 estimation in a SCR. SAE Tech. Pap. Ser. 2013-01-1581 (2013)
24. Watling, T.C., Tutuianu, M., Desai, M.R., Dai, J., Markatou, P., Johansson, A.: Development and validation of a Cu-Zeolite SCR catalyst model. SAE Tech. Pap. Ser. 2011-01-1299 (2011)